Design principles of fluoroether solvents for lithium metal battery electrolytes unveiled by extensive molecular simulation and machine learning

Xueying Yuan,[†] Xiupeng Chen,[†] Yuanxin Zhou,[†] Zhiao Yu,[‡,¶] and Xian Kong[*,†,§]

[†]*South China Advanced Institute for Soft Matter Science and Technology, School of Emergent Soft Matter, South China University of Technology, Guangzhou 510640, China*

[‡]*Department of Chemical Engineering, Stanford University, Stanford, CA 94305, USA*

[¶]*Present address: Feon Energy Inc., Woburn, Massachusetts 01801, USA*

[§]*Guangdong Provincial Key Laboratory of Functional and Intelligent Hybrid Materials and Devices, South China University of Technology, Guangzhou 510640, China*

E-mail: xk@scut.edu.cn

Abstract

Electrolyte engineering with fluoroether as solvents offers promising potential for high-performance lithium metal batteries. Despite recent progresses achieved in designing and synthesizing novel fluoroether solvents, a systematic understanding of how fluorination patterns impact electrolyte performance is still lacking. We investigate the effects of fluorination patterns on fluorinated 1,2-diethoxyethane (FDEE) as electrolyte solvents. By employing quantum calculations, molecular dynamics simulations, and interpretable machine learning, we establish significant correlations between fluorination patterns and electrolyte properties. Higher fluorination levels enhance FDEE stability

but decrease conductivity. The symmetry of fluorination sites is critical for stability and viscosity, while exerting minimal influence on ionic conductivity. FDEEs with highly symmetric fluorination sites exhibit favorable viscosity, stability, and overall electrolyte performance. Conductivity primarily depends on lithium-anion dissociation or association. These findings provide design principles for rational fluoroether electrolyte design, emphasizing the trade-offs between stability, viscosity, and conductivity. Our work underscores the significance of considering fluorination patterns and molecular symmetry in the development of electrolytes for advanced lithium metal batteries.

Introduction

Lithium metal batteries (LMBs), often considered as the prospective energy storage solution for the future due to their high theoretical specific energy,[1,2] are confronted with a significant drawback of poor cycling stability. This issue stems from the uncontrolled growth of dendrites and the fragile nature of the solid-electrolyte interphase (SEI) formed on the surface of lithium metal anodes.[3,4] A myriad of strategies have been extensively investigated to mitigate the instability issues encountered in LMBs. These strategies encompass the utilization of host materials with novel structures,[5–8] artificial coatings on lithium metal anode,[9–14] solid-state electrolytes,[15–18] optimized cycling protocols,[19] and electrolytes engineering.[20–22] Notably, among these methods, liquid electrolytes engineering proves to be a cost-effective approach,[23–25] considering their widespread employment in current commercial lithium-ion batteries, and their direct contact with all other battery components.[26]

By tuning the constituents of liquid electrolytes, it becomes possible to regulate both the chemistry of the solid-electrolyte interphase (SEI) and the morphology of lithium deposition, thus enabling more stable cycling of LMBs. For instance, studies have demonstrated that high-concentration electrolytes, with salt concentrations $\geq$ 4 M, enhance battery stability by suppressing the growth of lithium dendrites through a restructuring of the ion solvation shell.[27–29] In a similar vein, localized high-concentration electrolytes have been developed,

in which a weakly solvating or non-solvating co-solvent is introduced to maintain an ion solvation shell that mimics the effects of high-concentration electrolytes at salt concentrations around 1-2 M. These localized high-concentration electrolytes exhibit a stabilizing effect comparable to that of high-concentration electrolytes, while maintaining low viscosity, high conductivity, and cost-effectiveness.[30,31] Furthermore, other optimization approaches for liquid electrolytes have also proven effective, such as the incorporation of additives,[32–34] the utilization of liquefied gas electrolytes,[35–37] and the exploration of new solvent molecules,[38–42] among others.

Over the years, two key features of high-performance liquid electrolytes enabling LMBs are recognized. Firstly, it is important that the solvents do not strongly coordinate with lithium-ion (Li^+). In electrolytes with weak solvation ability, Li^+ is more likely to be coordinated with anions. This results in increased anion decomposition at the lithium metal anode, leading to the formation of an inorganic-rich SEI with beneficial mechanical and electrochemical properties, thereby improving the cycling performance of LMBs.[43] Furthermore, the charge transfer reaction of Li^+ in a weak solvation environment necessitates a less negative Li/Li^+ equilibrium potential and hence higher surface energy of Li metal. This favors more uniform deposition.[44] However, it is crucial to avoid excessively weak solvation as it results in low salt solubility, leading to insufficient ion conductivity. Secondly, the presence of a substantial amount of fluorine element in the electrolytes, whether in solvents, anions, or additives, is beneficial.[45–49] Although the underlying mechanism is not yet fully understood,[50–52] inorganic fluorides, primarily LiF, are recognized as important components of the SEI. They facilitate uniform lithium deposition and improve the performance of the lithium metal anode.[26,34,53,54] Increasing the abundance of fluorine in electrolytes enhances the formation of LiF, thus promoting the desired effects.

Recently, fluoroethers, or fluorinated ethers, have emerged as promising solvents for improving the performance of LMBs. Fluoroethers not only possess the aforementioned desirable characteristics, but also exhibit additional attributes that enhance their practical

viability in LMB applications. Firstly, fluorine, being the most electronegative element, enhances the oxidative stability of molecules upon fluorination. This property is particularly advantageous for ether-based solvents. Traditional ether-based solvents have shown benefits for lithium metal anodes; however, their limited oxidative stability against cathodes has hindered their widespread adoption.[55] Secondly, the inclusion of fluoro-groups in fluoroethers exhibits a strong electron-withdrawing effect, reducing the electron density on oxygen atoms. As a result, the polarity and solvation ability of the ether oxygen atoms are weakened. This effect yields similar advantages as observed in high-concentration electrolytes or localized high-concentration electrolytes. Additionally, fluoro-groups typically possess sufficient polarity to provide a comparable solvating ability to that of ether oxygen atoms.[38,39,41] Put differently, the presence of fluoro-groups in fluoroethers counteracts the reduced solvation ability of ether oxygen atoms by introducing additional solvation sites. This compensates for the weakened polarity of the ether oxygen atoms, ensuring sufficient salt solubility and promoting desirable ionic conductivity. Last but not least, fluoroethers enable the design of single-salt-single-solvent electrolytes (4SEs), which consist of a single solvent and a standard-concentration single salt. While they may not offer the versatility and synergistic effects of multi-salt or multi-solvent electrolytes,[56] 4SEs eliminate the need for formulation optimization and the alignment of electrochemical windows among different components.[57] As a result, the design and production processes are greatly simplified. Consequently, 4SEs can serve as model systems that facilitate more comprehensive investigations into solvation effects and the structure-function relationship in electrolytes.

In recent years, significant advancements have been made in the synthesis of novel and purposefully designed fluoroether solvents, demonstrating their tremendous potential in enabling practical LMBs.[38,39,41,55,58] These studies have underscored the possibility of enhancing electrolyte performance through the synthesis of new chemical compounds. However, despite the remarkable progress achieved through the exploration of several (approximately 10) new fluoroethers, the molecular-level design principles governing the behavior of fluo-

roether solvents remain elusive.[23] Specifically, the influence of fluorination sites on chemical stability, ion solvation, and ion transport mechanisms remains unknown. Meanwhile, it has been demonstrated that even slight modifications in the molecular structure of fluoroether solvents can lead to significant improvements in electrolyte performance. For instance, despite all being fluorinated-1,2-diethoxyethanes (fluorinated-DEEs), F3DEE and F6DEE do not perform as well as F4DEE and F5DEE.[39]

Given the vast number of potential fluoroether molecules, it is impractical to synthesize and test them individually. Therefore, there is an urgent need for a deeper understanding of the design principles governing fluoroethers, as well as the development of rapid screening methods for identifying promising candidate fluoroethers. In recent decades, significant progress has been made in the field of molecular simulations,[59,60] allowing for accurate predictions of diverse electrolyte properties. Consequently, this advancement has emerged as an efficient approach for understanding, designing, and screening electrolytes.[61–67] Moreover, the advent of machine learning (ML) has revolutionized the landscape of technology and scientific research.[68–71] ML offers promising avenues to unveil previously elusive principles and facilitates high-throughput screening of materials, thus accelerating progress in various fields.[72–75]

In this study, we aim to address the aforementioned knowledge gaps by developing a comprehensive workflow that combines molecular simulations and machine learning (ML) techniques. To begin, we select DEE as the template backbone solvent molecule due to the availability of preliminary experimental data on the effects of fluorination sites in DEE.[39] Our approach involves the exhaustive generation of all possible fluorinated DEE (FDEE) molecules with up to six fluorination sites. For each FDEE, we employ quantum density functional theory (DFT) calculations and classical molecular dynamics (MD) simulations to estimate its electrochemical stability window, viscosity, and ionic conductivity of LiFSI electrolytes. The results obtained from the DFT and MD simulations are then subjected to ML analysis to elucidate the impact of fluorination sites on various electrolyte properties.

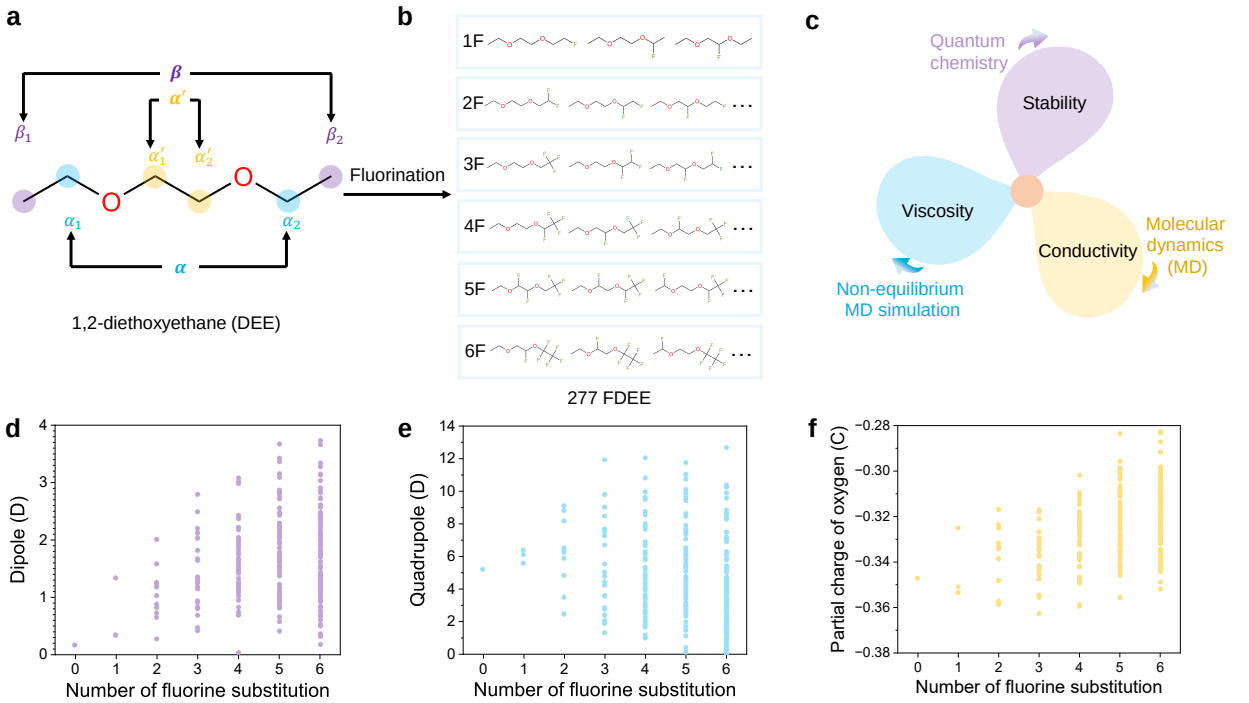

Figure 1: Computational design and screening of fluorinated-1,2-diethoxyethane (FDEE) for electrolytes solvent. a, Molecular structure of DEE and the nomenclature of available fluorination sites. b, 277 FDEE molecules with 1 to 6 fluorine atoms are generated. c, Key factors affecting electrolytes performance are evaluated. The factors include oxidation and reduction stability, viscosity, and ionic conductivity. d-f, The influence of fluorination degree on molecular dipole (d), quadrupole (e), and the partial charge of ether oxygen atoms (f).

Additionally, we delve into a more detailed investigation of Li^+ solvation in electrolytes based on a selection of representative FDEEs. This analysis aims to provide a deeper understanding of the underlying mechanisms at play. Importantly, the proposed workflow is based on widely available simulation methods and provides universal guidelines for future solvent molecule design and high-throughput screening.

Results

Generating fluorinated DEE molecules

A DEE molecule comprises six saturated carbons that serve as potential fluorination sites. These sites are denoted as $\beta_1, \alpha_1, \alpha_1', \alpha_2', \alpha_2$, and β_2 as shown in Figure 1a. In this study,

without bothering about the difficulties in synthesis, we have exhaustively generated all possible fluorinated DEEs (FDEEs) with a maximum of six fluorine atoms, as illustrated in Figure 1b and Supplementary Figure S1. Remarkably, even when considering DEE as the sole template molecule, this fluorination process has yielded 277 distinct chemically unique FDEE molecules. The number of candidate fluoroether solvents increases exponentially when considering other template molecules, making the options practically countless.

The generated FDEEs can be subjected to standard DFT calculations and MD simulations as depicted in Figure 1c and detailed in subsequent sections, to investigate their chemical and electrochemical properties (see Table S1). Prior to conducting computationally intensive calculations, we first examine computationally straightforward metrics. After generating the configuration of an FDEE molecule, charges are assigned using the electronegativity equalization method (eem).[76] This enables the estimation of molecular properties, including dipole, quadrupole, and partial charges (Figures 1 d-f).

Analysis of molecular dipoles reveals a weak increasing trend and an expanded distribution as the number of fluorine atoms increases from 1 to 6. In comparison, the trend in quadrupole is less apparent. The number of fluorine atoms in FDEEs can lead to either an increase or decrease in the molecule's quadrupole, resulting in a more dispersed distribution. The magnitudes of oxygen partial charges exhibit a slight decrease as the number of fluorine atoms increases. Nevertheless, these trends are obscured by significant variations within the distributions.

These observations indicate that the effects of fluorination cannot be adequately characterized solely by the number of fluorine atoms. Instead, it is necessary to consider specific details of the fluorination conditions, such as the positions of fluorination sites.

Chemical stability

To assess the chemical stability of FDEEs, we performed calculations of their Highest Occupied Molecular Orbitals (HOMOs) and Lowest Unoccupied Molecular Orbitals (LUMOs)

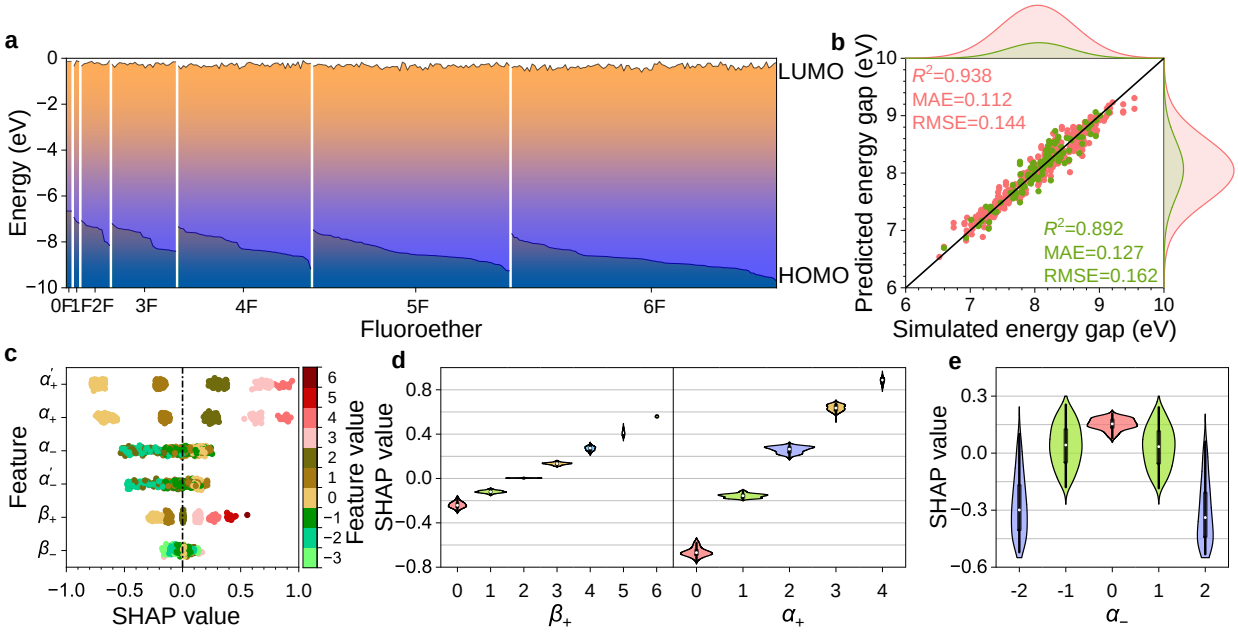

Figure 2: Chemical stability of FDEEs. a, Distribution of HOMO/LUMO energies for FDEEs with varying degrees of fluorination. b, Performance of machine learning in predicting the energy gap, represented by the training and test set data (red and green dots, respectively). c, SHAP values for all input features, providing local interpretability of the machine learning model. d, Dependence of SHAP values on β_+ and α_+. e, Dependence of SHAP values on α_-.

using Density Functional Theory (DFT), as described in the methods section. As shown in Figure 2a, the LUMOs of FDEEs exhibit minimal variation with the degree of fluorination. In contrast, as the degree of fluorination increases, there is a slight decreasing trend in the HOMO values. However, it is important to note that the range of HOMO values for FDEEs with the same number of fluorinated sites is quite extensive. This finding indicates that the specific fluorination sites play an equally significant role in determining the chemical stability of FDEEs, consistent with the behaviors observed in terms of dipole, quadrupole, and oxygen partial charge in the last section.

To investigate the relationship between fluorination sites and stability, we employed machine learning (ML) techniques. In particular, we trained a multilayer perceptron (MLP) to establish a correlation between the fluorination sites and the energy gap, which is quantified by the difference between the HOMO and the LUMO. Further details regarding this

methodology can be found in the methods section. In our MLP model, the inputs are the number of fluorine (F) atoms attached to each carbon atom in FDEEs. These inputs are also denoted as $\beta_1, \alpha_1, \alpha_1', \alpha_2', \alpha_2$, and β_2, without any confusion. These labels allow us to precisely identify the fluorination sites in the molecule, which are crucial for the subsequent ML analysis.

To enhance the meaningfulness of the inputs, we introduce linear combinations of the fluorination sites as new input features,

$$\alpha_+ = \alpha_1 + \alpha_2,\ \alpha_- = \alpha_1 - \alpha_2 \tag{1}$$

$$\alpha'_+ = \alpha'_1 + \alpha'_2,\ \alpha'_- = \alpha'_1 - \alpha'_2 \tag{2}$$

$$\beta_+ = \beta_1 + \beta_2,\ \beta_- = \beta_1 - \beta_2 \tag{3}$$

While the sum features (α_+, α'_+, β_+) tell the total number of fluorine atoms at corresponding sites, the difference features (α_-, α'_-, β_-) reflect the degree of symmetry (or asymmetry) due to fluorination at the corresponding sites.

The trained MLP model demonstrates fair performance in predicting the energy gap (Figure 2b). This suggests that the variation in the energy gap upon fluorination follows rules that can be decently captured by the model. To gain further chemical insights and understand the importance of each input feature, we conducted Shapley-additive-explanation (SHAP) analysis. SHAP analysis provides a quantitative measurement of the contribution of each feature to the predicted output for each sample, allowing for local interpretability of the ML model.[77] By analyzing the SHAP values, we can assess the significance and impact of individual features on the energy gap predictions.

Figure 2c shows the distribution of SHAP values for all features across all samples, ranked by their importance from top to bottom. Obviously, the spread of SHAP values is broader for features involving α or α', suggesting that the energy gap is more sensitive to fluorination at α or α' sites compared to β sites. This observation aligns with chemical intuition, as β

sites are farther away from the ether oxygens. Additionally, the distributions of SHAP values for α_+ and α'_+ are nearly identical, suggesting that fluorination at α or α' sites has an equal effect on the energy gap. Another noteworthy observation is that the SHAP value exhibits a monotonic increase with respect to all three sum features: α_+, $\alpha'+$, and $\beta+$. These sum features represent the number of fluorination sites, indicating that an increased number of fluorination sites leads to a larger energy gap,[45] as also demonstrated by the overall trend in Figure 2a. Analyzing the relationship between SHAP values and the sum features, we find a nearly linear increase, as depicted in Figure 2d and Figure S2a. The slopes for α_+ and α'_+ are larger compared to that of β_+, underscoring the dominant influence of α and α' fluorinations.

The relationship between the energy gap and the difference features, namely α_- (Figure 2e), α'_- (Figure S2b), and β_- (Figure S2c), exhibits a non-trivial behavior that has not been previously observed or reported. The corresponding SHAP values decrease as the absolute value of the corresponding feature increases, although the trend is less pronounced for β_-. This finding suggests that symmetric fluorination at chemically identical sites favors an increased energy gap. The underlying reason for this trend is likely due to the fact that more asymmetric fluorination results in a higher number of fluorine atoms on a particular site, leading to a more pronounced electron withdrawal from the neighboring ether oxygen atom. This electron withdrawal can induce chemical instability, thereby influencing the energy gap.

Viscosity of pure FDEE solvent

Viscosity plays a pivotal role in the characterization of liquid electrolytes as it not only influences the transport behavior of ions but also affects the processability of electrolytes during battery assembly.[78–80] Viscosities of pure FDEE solvents were estimated using non-equilibrium MD simulations, as described in the Methods section and in Supplementary Information. The viscosity of pure FDEE solvents exhibits a non-monotonic dependence on the

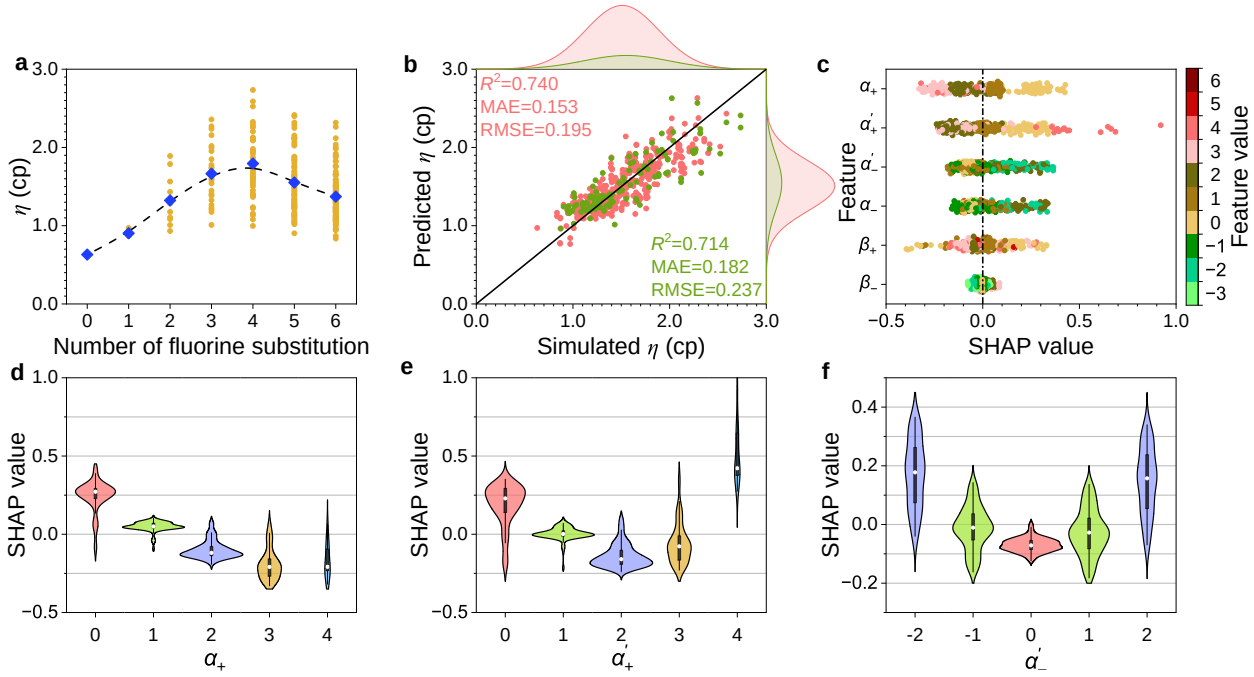

Figure 3: Viscosity of pure FDEE solvents. a, Distribution of viscosity for FDEEs with varying degrees of fluorination. b, Performance of machine learning in predicting the viscosity, represented by the training and test set data (red and green dots, respectively). c, SHAP values for all input features, providing local interpretability of the machine learning model. d-f, Dependence of SHAP values on different input features: α_+ (d), α'_+ (e), α'_- (f).

fluorination degree, as shown in Figure 3a. Prior to the 4-site fluorination, a slight increase in viscosity is observed with the fluorination degree. However, beyond this point, the viscosity shows a decreasing trend with a higher fluorination degree (Figure 3a). This non-monotonic behavior reflects the trade-off between two potentially competing factors associated with fluorination: intermolecular interactions and bulkiness. With a higher fluorination degree, the polarity and intermolecular interactions of FDEEs strengthen, as indicated by the more negative cohesive energy (Figure S3a). This enhanced inter-molecular interaction flattens after 4-site fluorination (Figure S3a), which corresponds to the trend observed in the viscosity as the fluorination degree increases. Enhanced intermolecular interaction contributes to the increase of viscosity (Figure S3b).[80] On the other hand, the fluorination of FDEEs leads to increased bulkiness, resulting in a less compact arrangement of molecules. This is supported by the observed increase in molar volume with higher fluorination degree (Figure

S4a), which is expected due to the larger size of fluorine compared to hydrogen. The looser packing of molecules has a slightly favorable influence on reducing viscosity (Figure S4b). Therefore, the non-monotonic trend observed in the viscosity of FDEEs can be attributed to the delicate balance between these two competing factors.

Machine learning is employed to establish the relationship between viscosity and fluorination sites. The trained ML model (Figure 3b) exhibits a lower prediction performance compared to the case of chemical stability. The mean absolute error (MAE) is 0.153 and 0.182 for the training set and test set, respectively. The larger prediction error, in contrast to the energy gap, suggests that viscosity is not solely determined by the chemical structure of the FDEEs. Other factors such as intermolecular interactions, spatial effects, and electronic repulsion also play significant roles in governing the viscosity.

Nevertheless, the SHAP analysis of the ML model for viscosity prediction still furnishes valuable insights into the impact of fluorination on viscosity. In contrast to the ML model for energy gap prediction, the SHAP values for all features, except for β_-, exhibit comparable ranges (Figure 3c). This indicates that there are no single dominant fluorination features that solely determine viscosity.

The SHAP analysis reveals distinct dependencies of the SHAP values on α_+ and α'_+ features. For α_+, the SHAP value shows a steady decrease with increasing fluorination at α-sites (Figure 3d), indicating that additional fluorination at these sites contributes to reducing viscosity. In contrast, the SHAP value exhibits a non-monotonic dependence on α'_+, initially decreasing until $\alpha'_+ = 2$, and then increasing thereafter (Figure 3e). Excessive fluorination at α'-sites leads to higher viscosity, potentially attributed to increased molecular rigidity. This can be observed in Figure S5a, where the distribution of the dihedral angle formed by O-Cα'-Cα'-O (φ) becomes more biased as α'_+ values increase, except for $\alpha'_+ = 4$. This indicates a higher likelihood of the dihedral angle being trapped in energetically favorable configurations, suggesting reduced flexibility. The autocorrelation function of φ in Figure S5b,c further supports this finding, as larger α'_+ values, except for $\alpha'_+ = 4$, exhibit longer

correlation times for φ. A concrete explanation for the high viscosity at $\alpha'_+ = 4$ situation is still elusive. The relatively large SHAP values observed in Figure 3e may be attributed to the noise introduced by the small sample size (there are only nine chemically unique FDEE molecules with $\alpha'_+ = 4$). While the packing density barely show dependence on α'_+ value (Figure S6a), the more negative cohesive energy for FDEEs with $\alpha'_+ = 4$ than other FDEEs suggests enhanced interaction among molecules (Figure S6b), which provide a plausible alternative explanation for a notable rise in viscosity when $\alpha'_+ = 4$ (Figure S6c).

The fluorination at the β position away from the oxygen has little effect on the viscosity (Figure S7a-b), obviously due to their large distance from the ether oxygen. The SHAP values show similar dependencies on α'_- (Figure 3f) and α_- (Figure S7c), indicating that larger absolute values of these difference features are associated with higher viscosity. This suggests that increased asymmetry in fluorination patterns contributes to higher viscosity. A molecule with greater asymmetry tends to have a higher molecular dipole, resulting in stronger intermolecular interactions and, consequently, higher viscosity.

Ionic conductivity

The primary function of electrolytes is to facilitate the conduction of ionic charges, which is quantitatively assessed by the metric of ionic conductivity. To evaluate the impact of fluorination on the ionic conductivity of FDEE-based electrolytes, we performed molecular dynamics (MD) simulations of electrolytes containing 1.2 M LiFSI dissolved in FDEE solvents. The ionic conductivities were determined by calculating the Onsager transport coefficients, which provide a measure of the correlations in the transport between ions. Detailed information on the simulation and analysis methods can be found in the Methods section.

Figure 4a illustrates the conductivity of single-ion-single-solvent electrolytes utilizing FDEEs. Evidently, an increase in fluorination leads to a decrease in conductivity, which aligns with existing experimental findings.[39,55] According to conventional knowledge, this

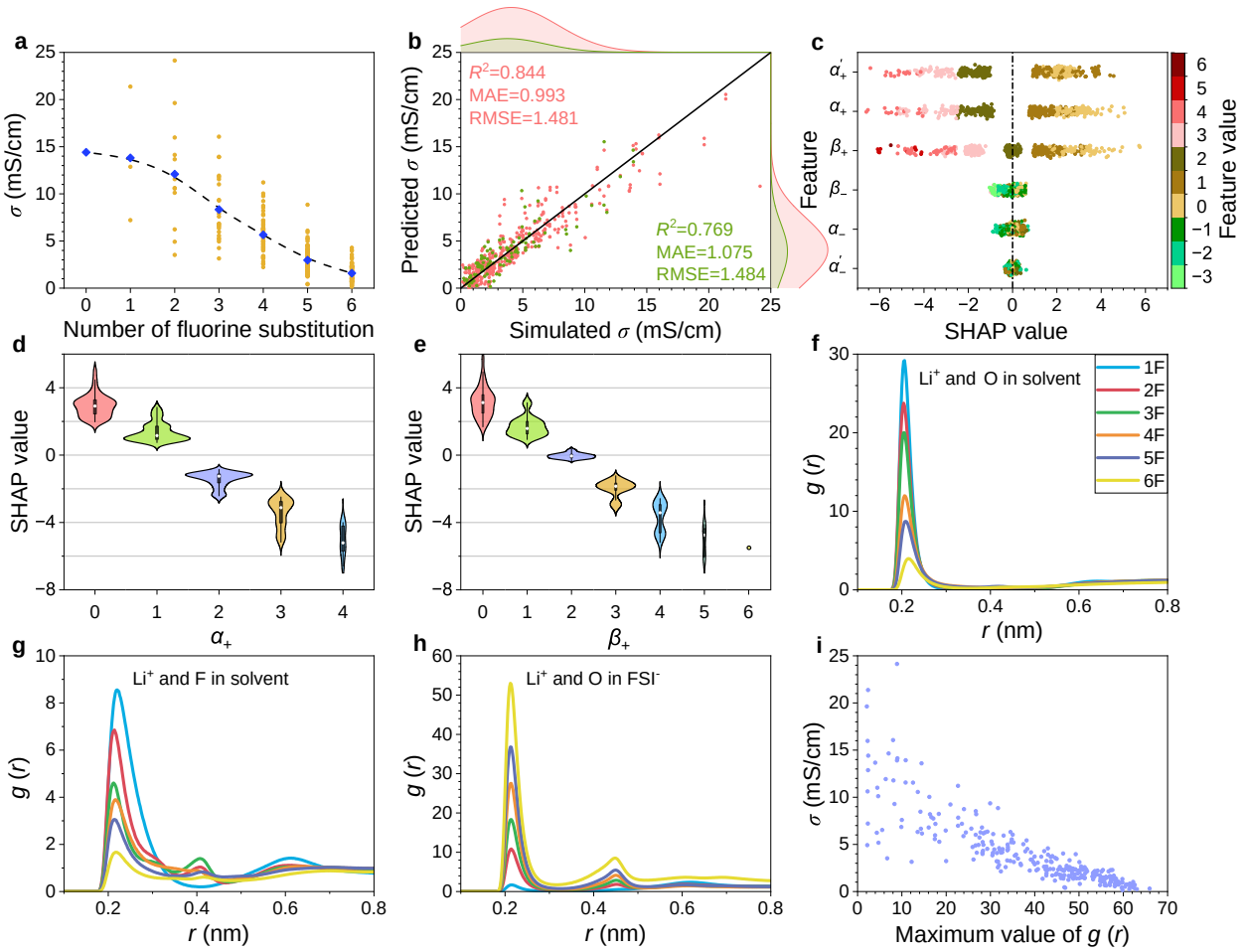

Figure 4: Ionic conductivity of 1.2 M LiFSI electrolytes with FDEE as solvent. a, Distribution of ionic conductivity for electrolytes with FDEEs of varying degrees of fluorination. b, Performance of machine learning in predicting the conductivity, represented by the training and test set data (red and green dots, respectively). c, SHAP values for all input features, providing local interpretability of the machine learning model. d-e, Dependence of SHAP values on different input features: α_+ (d), β_+ (e). f-h, Radial distribution functions $g(r)$'s between Li^+ and major solvating sites in FDEE and FSI for electrolytes with representative FDEEs: (f) oxygen in FDEE, (g) fluorine in FDEE, (h) oxygen in FSI. (i) Scatter plot between ionic conductivity and the first peak magnitude in the radial distribution function between Li^+ and oxygen in FSI $g(r_{max})$.

decline in conductivity is attributed to the elevated viscosity of the solvent.[81,82] However, as demonstrated in the above section, the viscosity of the solvent shows no significant increase once the number of fluorine exceeds four. The scattering plot between viscosity and ionic conductivity (Figure S8) shows no significant correlations. As we will show below, the actual reason behind the decline in ionic conductivity with increasing fluorination numbers is the

heightened ionic association or, equivalently, reduced ionic dissociation.

Similar to the case of viscosity, the performance of the trained ML model in predicting conductivity is only modest (Figure 4b). This indicates that the ionic conductivity is influenced by additional factors beyond the fluorination state, such as the interactions between FDEE molecules and ions, as well as the interactions among ions themselves. As depicted in Figure 4c, the range of SHAP values associated with different features provides clear evidence that the conductivity is primarily governed by the degree of fluorination. The increase in all sum features, namely α_+, β_+, and α'_+, leads to a comparable decrease in conductivity, as demonstrated in Figures 4d-e, and S9a. This insensitivity to the specific fluorination sites highlights the fact that Li^+ is only sensitive to the local structure of an FDEE molecule and its immediate surroundings.

The symmetry of fluorination does not play a significant role due to the relatively short-range interaction between an FDEE molecule and an ion, particularly Li^+. In other words, Li^+ does not interact with the entire FDEE molecule, but rather with specific regions or sites. Despite this fact, smaller absolute values of α_-, α'_-, and β_- are generally more favorable for conductivity, as shown in Figures S9b-d. This suggests that symmetrical fluorination can have a positive impact on conductivity, although its effects may be relatively weaker compared to the overall fluorination degree. Another notable observation is that conductivity is less sensitive to the asymmetry at α' sites. This can be attributed to the proximity of the two α' sites, namely α'_1 and α'_2. As a result, a Li^+ ion can interact with both α' sites simultaneously, leading to a reduced impact of individual asymmetry on conductivity.

To gain further insights into the conductivity of electrolytes based on different FDEEs, we investigate the solvation structure of Li^+ ions. Figure 4f-g present the radial distribution functions (RDFs) between Li^+ ions and oxygen or fluorine atoms in solvent molecules for several representative FDEEs. The RDFs reveal that both oxygen and fluorine atoms in FDEEs contribute to the solvation of Li^+ ions, consistent with previous findings.[38,39] As the fluorination degree increases, the peaks in the RDFs decrease for both oxygen and fluorine

atoms in FDEEs, indicating a reduced involvement of the solvent in Li^+ solvation. The magnitude of partial charges on oxygen atoms slightly decreases with increasing fluorination degree (Figure 1f), weakening the attraction between oxygen atoms and Li^+ ions.

To compensate for the reduced solvation by FDEEs, the solvation from anions becomes crucial. In Figure 4h, the RDFs between Li^+ ions and oxygen atoms in anions are shown for representative FDEEs with varying fluorination degrees. The RDF exhibits two peaks: the first peak at $r = 0.22$ nm corresponds to the direct contact between lithium ion and FSI, which exist in contact ion pairs (CIPs) and ion clusters; the second peak at $r = 0.45$ nm corresponds to lithium ion and FSI separated by either solvent (as in solvent-separated ion pairs, SSIPs) or another ion (as in ion clusters). It is evident that FDEEs with higher fluorination degrees exhibit stronger associations between Li^+ and anions and a lower dissociation degree (Table S3). Ion cluster analysis shows that larger clusters are more likely to form in FDEEs with high fluorination degree (Figure S10). Ion pairs and neutral ion clusters do not contribute to ionic conductivity since they do not facilitate the transport of net charge carriers. This findings indicate that the deterioration in ionic conductivity observed with increasing fluorination degree in FDEEs can be predominantly attributed to heightened ionic association. It is well-established that such association can lead to transport anomalies in electrolytes.[83,84] To further validate this observation, we quantify the association between Li^+ ions and anions by measuring the magnitude of the first peak in the RDF, denoted as $g(r_{\max})$, and correlate it with the ionic conductivity (Figure 4i). The trend depicted in the plot confirms that strong ionic association is the major factor responsible for the low ionic conductivity observed in FDEEs with higher fluorination degrees.

The contribution of different ionic movement correlations to the overall conductivity can be analyzed and decomposed. As described in the Supplementary Information, the conductivity in our studied systems can be computed using the equation $\sigma = F^2(L^{++}+L^{--}-2L^{+-})$, where F represents Faraday's constant. The Onsager transport coefficients (L^{ij}'s, with i and j denote ionic species) provide insights into the relative importance of various ionic corre-

lations. Specifically, L^{++} characterizes the correlated motions among cations, including self-correlations and cross-correlations, while L^{+-} quantifies the correlations between cation and anion movements. Figure S11a illustrates the Onsager transport coefficients for electrolytes containing different fluoroether solvents (FDEEs). It is observed that all L^{ij} values exhibit a slight increase with increasing fluorination degree, albeit with larger fluctuations. Since the difference between L^{+-} and either L^{++} or L^{--} determines the conductivity, we further examine the correlations among L^{ij} values (Figures S11b-c). When the L^{ij} values are small, L^{+-} is slightly smaller than both L^{++} and L^{--}, indicating that the correlation between cation and anion movements is smaller compared to the correlations between ions of the same type, which is conducive to higher conductivity. This also suggests a relatively high degree of ion dissociation. At higher values of L^{ij}, both L^{++} and L^{--} exhibit strong positive correlations with L^{+-}, and the difference between them diminishes. This trend reflects the formation of ion pairs and clusters, which is more likely to occur in electrolytes containing FDEEs with high fluorination degrees. The increase in L^{ij} values is associated with ion association, as evidenced by the positive correlation between L^{+-} and $g(r_{\max})$ (Figure S12).

Screening of optimal FDEEs

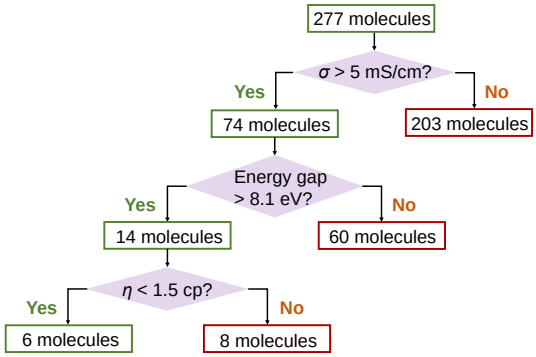

Figure 5: According to the average of the predicted values of conductivity (4.063 mS/cm), energy gap (8.045 eV) and viscosity (1.510 cp) in machine learning, six candidate solvents were selected out.

From the above discussions, it is evident that fluorination introduces competing effects on

Table 1. Six candidate solvent molecules and their performance

Name [a]	SMILES	Viscosity (cp)	Conductivity (mS/cm)	Energy gap (eV)
C13	C(F)COC(F)COC(F)C	1.226	13.902	8.248
C23	CC(F)OC(F)COC(F)C	1.326	11.550	8.145
C22	CC(F)OC(F)C(F)OCC	1.206	9.355	8.125
E59	C(F)C(F)OC(F)COC(F)C(F)	1.394	8.847	8.532
D29	C(F)C(F)OCC(F)OC(F)C	1.408	8.525	8.177
D37	C(F)COC(F)C(F)OC(F)C	0.997	5.023	8.152

[a] ID code for each FDEE (see Supplementary Table S1). Here, A, B, C, D, E, and F represent DEE being substituted by 1F, 2F, 3F, 4F, 5F, and 6F.

the ionic conductivity and electrochemical stability of FDEE solvents. Specifically, increased fluorination tends to enhance stability but comes at the cost of reduced ionic conductivity. This dilemma highlights the inherent trade-off that must be considered when designing or selecting FDEE solvents. It emphasizes the need for high-throughput simulation and screening approaches in the design of fluorinated electrolytes since there are no straightforward rules to guide experimental rational design. The complex interplay between fluorination and solvent properties underscores the importance of computational methods to explore and understand the intricate relationships between structure, properties, and performance in electrolyte design.

To furnish experimental exploration of high-performance electrolytes based on FDEEs, we have identified six candidate FDEEs through a multi-stage screening process based on the calculated properties in our study, including ionic conductivity, energy gap, and viscosity (Figure 5 and Table 1). None of the six FDEEs screened in this study have been assigned a CAS number at this time. As anticipated, these six FDEEs adhere to the design principles outlined in the previous sections. Notably, these high-performing FDEEs share a common characteristic: they possess multiple single-fluorine modifications. These single-fluorine sites are strategically arranged to maximize the symmetry of the FDEEs, as symmetry has been

identified as a key factor in determining performance.[85] Further analysis, such as careful examination of the radial distribution functions (RDFs) between Li^+ and the anion or oxygen in FDEEs (Figures S13a-b), supports the rule that a high degree of ion dissociation contributes to enhanced ionic conductivity. These findings provide evidences that validate the design principles derived from our computational investigations.

Conclusions

In conclusion, our comprehensive study employed a combination of quantum calculations, molecular simulations, and machine learning to investigate the influence of fluorination patterns on a family of FDEE-based electrolytes, focusing on properties relevant to battery electrolytes such as chemical stability, viscosity, and conductivity. We established significant correlations between the fluorination patterns and the electrolyte properties. Our findings revealed that while high levels of fluorination generally enhance the stability of FDEE molecules, they also lead to decreased conductivity of the electrolytes. Importantly, the symmetry of the fluorination sites emerged as a crucial and often overlooked feature that strongly influences the stability and viscosity of FDEEs, while exerting minimal effects on the ionic conductivity. Highly symmetric fluorination sites were found to preserve low viscosity and high stability, thereby benefiting overall electrolyte performance. The conductivity was primarily determined by the degree of dissociation between lithium and the anion, or by the degree of association between them. Strong association resulted in fewer dissociated free charge carriers, leading to lower conductivity. By performing a multi-stage screening based on conductivity, stability, and viscosity, we identified potential candidates from the pool of FDEEs. These design rules are essential for the rational design of fluorinated ether-based electrolytes. The workflow we have established is versatile and can be readily adapted to investigate other families of electrolytes, enabling the design of high-performance electrolyte materials for various energy storage applications.

Methods

Generation of candidate FDEEs

A systematic generation of FDEEs that contain no more than six fluorination sites was performed using Openbabel 3.1.0[86] by manipulating the input SMILE codes. Due to the lack of unique mapping between SMILE codes and actual molecules, additional verification was carried out to eliminate chemically identical FDEE molecules. The resulting set of structures is presented in Supplementary Information Figure S1.

Density functional theory calculation

All DFT calculations were performed at the B3LYP/6-311++G** level. Prior to calculating the HOMO/LUMO energy levels, molecular geometries were optimized at the same level. The DFT calculations were carried out using ORCA 5.0.3 software.[87] Post-processing and analysis of the DFT calculations were performed using Multiwfn 3.7[88] and Visual Molecular Dynamics (VMD) 1.9.3.[89] To ensure the reliability of our methods, a benchmarking study of the HOMO/LUMO energy levels of typical electrolyte solvent molecules was conducted before the production calculations for all FDEEs. This involved exploring different combinations of functional and basis sets using various software and comparing the results with data reported in the literature. Further details can be found in Supplementary Information Table S3.

Molecular dynamics simulation

In molecular dynamics (MD) simulations, the interactions between atoms were described using the Optimized Potentials for Liquid Simulations all-atom (OPLS-AA) force field.[90,91] The partial charges of the FDEEs were calculated using the Electronegativity Equalization Method (EEM)[76] implemented in OpenBabel 3.1.0.[86] We compared several charge assignment methods and found that the estimation by EEM method is closest to the RESP charges

obtained from DFT calculations (see Supplementary Information Table S4). To account for the overestimation of electrostatic interactions, partial charges were scaled[92,93] by a factor to match experimental values (see Supplementary Information Figure S15). All MD simulations were performed using GROMACS 202203.[94] Further information can be found in Table S5.

The viscosities of pure FDEE solvents were determined using non-equilibrium molecular dynamics (MD) simulations.[95] The conductivity of LiFSI electrolytes with FDEE solvents was obtained through equilibrium MD simulations with 1.2 M solutions of LiFSI, utilizing the Onsager transport coefficients.[96,97] More details regarding viscosity and conductivity calculations can be found in section Viscosity calculation and Conductivity calculation in SI, respectively.

Machine learning

In this study, fully connected neural networks were employed to establish correlations between input features and various metrics of FDEEs. The multilayer perceptron (MLP) libraries[98] implemented in the scikit-learn Python package[99] were utilized for this purpose. Additionally, the SHAP (SHapley Additive exPlanations) package[77] was employed for the analysis of feature importance. Further information regarding the machine learning methodology, SHAP analysis, and hyperparameter optimizations can be found in Section Machine learning of the Supplementary Information.

Acknowledgement

This research has been supported by Guangdong Basic and Applied Basic Research Foundation (2022A1515110016) , the Recruitment Program of Guangdong (2016ZT06C322) and TCL Science and Technology Innovation Fund.

Author contributions

X.K. conceived the project and designed the research; X.Y., X.C., and Y.Z. performed research; X.Y., Z.Y., and X.K. discussed the results; X.Y. and X.K. wrote and edited the manuscript; all authors reviewed the manuscript.

Supporting Information Available

Supplementary information is available for this paper at https://

References

(1) Liu, J. et al. Pathways for practical high-energy long-cycling lithium metal batteries. *Nature Energy* **2019**, *4*.

(2) Lin, D.; Liu, Y.; Cui, Y. Reviving the lithium metal anode for high-energy batteries. *Nature Nanotechnology* **2017**, *12*, 194–206.

(3) Tikekar, M. D.; Choudhury, S.; Tu, Z.; Archer, L. A. Design principles for electrolytes and interfaces for stable lithium-metal batteries. *Nature Energy* **2016**, *1*, 16114.

(4) Cheng, X.-B.; Zhang, R.; Zhao, C.-Z.; Zhang, Q. Toward Safe Lithium Metal Anode in Rechargeable Batteries: A Review. *Chemical Reviews* **2017**, *117*, 10403–10473, PMID: 28753298.

(5) Lin, D.; Liu, Y.; Liang, Z.; Lee, H.-W.; Sun, J.; Wang, H.; Yan, K.; Xie, J.; Cui, Y. Layered reduced graphene oxide with nanoscale interlayer gaps as a stable host for lithium metal anodes. *Nature Nanotechnology* **2016**, *11*, 626–632.

(6) Chen, H.; Pei, A.; Wan, J.; Lin, D.; Vilá, R.; Wang, H.; Mackanic, D.; Steinrück, H.-G.;

Huang, W.; Li, Y.; Yang, A.; Xie, J.; Wu, Y.; Wang, H.; Cui, Y. Tortuosity Effects in Lithium-Metal Host Anodes. *Joule* **2020**, *4*, 938–952.

(7) Wang, H.; Lin, D.; Xie, J.; Liu, Y.; Chen, H.; Li, Y.; Xu, J.; Zhou, G.; Zhang, Z.; Pei, A.; Zhu, Y.; Liu, K.; Wang, K.; Cui, Y. An Interconnected Channel-Like Framework as Host for Lithium Metal Composite Anodes. *Advanced Energy Materials* **2019**, *9*, 1802720.

(8) Niu, C.; Pan, H.; Xu, W.; Xiao, J.; Zhang, J.-G.; Luo, L.; Wang, C.; Mei, D.; Meng, J.; Wang, X.; Liu, Z.; Mai, L.; Liu, J. Self-smoothing anode for achieving high-energy lithium metal batteries under realistic conditions. *Nature Nanotechnology* **2019**, *14*, 594–601.

(9) Li, N.-W.; Yin, Y.-X.; Yang, C.-P.; Guo, Y.-G. An Artificial Solid Electrolyte Interphase Layer for Stable Lithium Metal Anodes. *Advanced Materials* **2016**, *28*, 1853–1858.

(10) Zheng, G.; Wang, C.; Pei, A.; Lopez, J.; Shi, F.; Chen, Z.; Sendek, A. D.; Lee, H.-W.; Lu, Z.; Schneider, H.; Safont-Sempere, M. M.; Chu, S.; Bao, Z.; Cui, Y. High-performance lithium metal negative electrode with a soft and flowable polymer coating. *ACS Energy Lett.* **2016**, *1*, 1247–1255.

(11) Kong, X.; Rudnicki, P. E.; Choudhury, S.; Bao, Z.; Qin, J. Dendrite Suppression by a Polymer Coating: A Coarse-Grained Molecular Study. *Advanced Functional Materials* **2020**, *30*, 1910138.

(12) Lopez, J.; Pei, A.; Oh, J. Y.; Wang, G.-J. N.; Cui, Y.; Bao, Z. Effects of polymer coatings on electrodeposited lithium metal. *Journal of the American Chemical Society* **2018**, *140*, 11735–11744.

(13) Kim, M. S.; Ryu, J.-H.; Deepika,; Lim, Y. R.; Nah, I. W.; Lee, K.-R.; Archer, L. A.; Il Cho, W. Langmuir–Blodgett artificial solid-electrolyte interphases for practical lithium metal batteries. *Nature Energy* **2018**, *3*, 889–898.

(14) Weng, Y.-T.; Liu, H.-W.; Pei, A.; Shi, F.; Wang, H.; Lin, C.-Y.; Huang, S.-S.; Su, L.-Y.; Hsu, J.-P.; Fang, C.-C.; Cui, Y.; Wu, N.-L. An ultrathin ionomer interphase for high efficiency lithium anode in carbonate based electrolyte. *Nature Communications* **2019**, *10*, 5824.

(15) Wang, Y.; Zanelotti, C. J.; Wang, X.; Kerr, R.; Jin, L.; Kan, W. H.; Dingemans, T. J.; Forsyth, M.; Madsen, L. A. Solid-state rigid-rod polymer composite electrolytes with nanocrystalline lithium ion pathways. *Nature Materials* **2021**, *20*, 1255–1263.

(16) Manthiram, A.; Yu, X.; Wang, S. Lithium battery chemistries enabled by solid-state electrolytes. *Nature Reviews Materials* **2017**, *2*, 1–16.

(17) Kim, S.; Kim, J.-S.; Miara, L.; Wang, Y.; Jung, S.-K.; Park, S. Y.; Song, Z.; Kim, H.; Badding, M.; Chang, J., et al. High-energy and durable lithium metal batteries using garnet-type solid electrolytes with tailored lithium-metal compatibility. *Nature Communications* **2022**, *13*, 1–12.

(18) Bouchet, R.; Maria, S.; Meziane, R.; Aboulaich, A.; Lienafa, L.; Bonnet, J.-P.; Phan, T. N.; Bertin, D.; Gigmes, D.; Devaux, D., et al. Single-ion BAB triblock copolymers as highly efficient electrolytes for lithium-metal batteries. *Nature materials* **2013**, *12*, 452–457.

(19) Stefani, F.; Weier, T.; Gundrum, T.; Gerbeth, G. How to circumvent the size limitation of liquid metal batteries due to the Tayler instability. *Energy conversion and management* **2011**, *52*, 2982–2986.

(20) Zhang, J.-G.; Xu, W.; Xiao, J.; Cao, X.; Liu, J. Lithium Metal Anodes with Nonaqueous Electrolytes. *Chemical Reviews* **2020**, *120*, 13312–13348, PMID: 33174427.

(21) Fan, X.; Wang, C. High-voltage liquid electrolytes for Li batteries: progress and perspectives. *Chem. Soc. Rev.* **2021**, *50*, 10486–10566.

(22) Hobold, G. M.; Lopez, J.; Guo, R.; Minafra, N.; Banerjee, A.; Shirley Meng, Y.; Shao-Horn, Y.; Gallant, B. M. Moving beyond 99.9% Coulombic efficiency for lithium anodes in liquid electrolytes. *Nature Energy* **2021**, *6*, 951–960.

(23) Wang, H.; Yu, Z.; Kong, X.; Kim, S. C.; Boyle, D. T.; Qin, J.; Bao, Z.; Cui, Y. Liquid electrolyte: The nexus of practical lithium metal batteries. *Joule* **2022**, *6*, 588–616.

(24) Jie, Y.; Ren, X.; Cao, R.; Cai, W.; Jiao, S. Advanced Liquid Electrolytes for Rechargeable Li Metal Batteries. *Advanced Functional Materials* **2020**, *30*, 1910777.

(25) Li, M.; Wang, C.; Chen, Z.; Xu, K.; Lu, J. New Concepts in Electrolytes. *Chemical Reviews* **2020**, *120*, 6783–6819, PMID: 32022546.

(26) Meng, Y. S.; Srinivasan, V.; Xu, K. Designing better electrolytes. *Science* **2022**, *378*, eabq3750.

(27) Qian, J.; Henderson, W. A.; Xu, W.; Bhattacharya, P.; Engelhard, M.; Borodin, O.; Zhang, J.-G. High rate and stable cycling of lithium metal anode. *Nature Communications* **2015**, *6*, 1–9.

(28) Yamada, Y.; Wang, J.; Ko, S.; Watanabe, E.; Yamada, A. Advances and issues in developing salt-concentrated battery electrolytes. *Nature Energy* **2019**, *4*, 269–280.

(29) Wang, J.; Yamada, Y.; Sodeyama, K.; Chiang, C. H.; Tateyama, Y.; Yamada, A. Superconcentrated electrolytes for a high-voltage lithium-ion battery. *Nature Communications* **2016**, *7*, 1–9.

(30) Chen, S.; Zheng, J.; Mei, D.; Han, K. S.; Engelhard, M. H.; Zhao, W.; Xu, W.; Liu, J.; Zhang, J.-G. High-Voltage Lithium-Metal Batteries Enabled by Localized High-Concentration Electrolytes. *Advanced Materials* **2018**, *30*, 1706102.

(31) Ren, X. et al. Enabling High-Voltage Lithium-Metal Batteries under Practical Conditions. *Joule* **2019**, *3*, 1662–1676.

(32) Zhang, H.; Eshetu, G. G.; Judez, X.; Li, C.; Rodriguez-Martínez, L. M.; Armand, M. Electrolyte Additives for Lithium Metal Anodes and Rechargeable Lithium Metal Batteries: Progress and Perspectives. *Angewandte Chemie International Edition* **2018**, *57*, 15002–15027.

(33) Qian, J.; Xu, W.; Bhattacharya, P.; Engelhard, M.; Henderson, W. A.; Zhang, Y.; Zhang, J.-G. Dendrite-free Li deposition using trace-amounts of water as an electrolyte additive. *Nano Energy* **2015**, *15*, 135–144.

(34) Zhang, X.-Q.; Cheng, X.-B.; Chen, X.; Yan, C.; Zhang, Q. Fluoroethylene Carbonate Additives to Render Uniform Li Deposits in Lithium Metal Batteries. *Advanced Functional Materials* **2017**, *27*, 1605989.

(35) Rustomji, C. S.; Yang, Y.; Kim, T. K.; Mac, J.; Kim, Y. J.; Caldwell, E.; Chung, H.; Meng, Y. S. Liquefied gas electrolytes for electrochemical energy storage devices. *Science* **2017**, *356*, eaal4263.

(36) Yang, Y.; Davies, D. M.; Yin, Y.; Borodin, O.; Lee, J. Z.; Fang, C.; Olguin, M.; Zhang, Y.; Sablina, E. S.; Wang, X.; Rustomji, C. S.; Meng, Y. S. High-Efficiency Lithium-Metal Anode Enabled by Liquefied Gas Electrolytes. *Joule* **2019**, *3*, 1986–2000.

(37) Ma, L.; Lee, J. Z.; Pollard, T. P.; Schroeder, M. A.; Limpert, M. A.; Craven, B.; Fess, S.; Rustomji, C. S.; Wang, C.; Borodin, O.; Xu, K. High-Efficiency Zinc-Metal Anode Enabled by Liquefied Gas Electrolytes. *ACS Energy Letters* **2021**, *6*, 4426–4430.

(38) Yu, Z.; Wang, H.; Kong, X.; Huang, W.; Tsao, Y.; Mackanic, D. G.; Wang, K.; Wang, X.; Huang, W.; Choudhury, S., et al. Molecular design for electrolyte solvents enabling energy-dense and long-cycling lithium metal batteries. *Nature Energy* **2020**, *5*, 526–533.

(39) Yu, Z.; Rudnicki, P. E.; Zhang, Z.; Huang, Z.; Celik, H.; Oyakhire, S. T.; Chen, Y.; Kong, X.; Kim, S. C.; Xiao, X., et al. Rational solvent molecule tuning for high-performance lithium metal battery electrolytes. *Nature Energy* **2022**, *7*, 94–106.

(40) Chen, Y.; Yu, Z.; Rudnicki, P.; Gong, H.; Huang, Z.; Kim, S. C.; Lai, J.-C.; Kong, X.; Qin, J.; Cui, Y.; Bao, Z. Steric Effect Tuned Ion Solvation Enabling Stable Cycling of High-Voltage Lithium Metal Battery. *Journal of the American Chemical Society* **2021**, *143*, 18703–18713, PMID: 34709034.

(41) Wang, H.; Yu, Z.; Kong, X.; Huang, W.; Zhang, Z.; Mackanic, D. G.; Huang, X.; Qin, J.; Bao, Z.; Cui, Y. Dual-solvent li-ion solvation enables high-performance Li-metal batteries. *Advanced Materials* **2021**, *33*, 2008619.

(42) Xu, R.; Ding, J.-F.; Ma, X.-X.; Yan, C.; Yao, Y.-X.; Huang, J.-Q. Designing and demystifying the lithium metal interface toward highly reversible batteries. *Advanced Materials* **2021**, *33*, 2105962.

(43) Kim, S. C.; Kong, X.; Vilá, R. A.; Huang, W.; Chen, Y.; Boyle, D. T.; Yu, Z.; Wang, H.; Bao, Z.; Qin, J.; Cui, Y. Potentiometric Measurement to Probe Solvation Energy and Its Correlation to Lithium Battery Cyclability. *Journal of the American Chemical Society* **2021**, *143*, 10301–10308, PMID: 34184873.

(44) Boyle, D. T.; Kim, S. C.; Oyakhire, S. T.; Vilá, R. A.; Huang, Z.; Sayavong, P.; Qin, J.; Bao, Z.; Cui, Y. Correlating Kinetics to Cyclability Reveals Thermodynamic Origin of Lithium Anode Morphology in Liquid Electrolytes. *Journal of the American Chemical Society* **2022**, *144*, 20717–20725, PMID: 36318744.

(45) Zhao, Y.; Zhou, T.; Ashirov, T.; Kazzi, M. E.; Cancellieri, C.; Jeurgens, L. P.; Choi, J. W.; Coskun, A. Fluorinated ether electrolyte with controlled solvation structure for high voltage lithium metal batteries. *Nature Communications* **2022**, *13*, 2575.

(46) Yoo, D.-J.; Liu, Q.; Cohen, O.; Kim, M.; Persson, K. A.; Zhang, Z. Rational Design of Fluorinated Electrolytes for Low Temperature Lithium-Ion Batteries. *Advanced Energy Materials* **2023**, 2204182.

(47) Chen, L.; Fan, X.; Hu, E.; Ji, X.; Chen, J.; Hou, S.; Deng, T.; Li, J.; Su, D.; Yang, X., et al. Achieving high energy density through increasing the output voltage: a highly reversible 5.3 V battery. *Chem* **2019**, *5*, 896–912.

(48) Cao, X.; Ren, X.; Zou, L.; Engelhard, M. H.; Huang, W.; Wang, H.; Matthews, B. E.; Lee, H.; Niu, C.; Arey, B. W., et al. Monolithic solid–electrolyte interphases formed in fluorinated orthoformate-based electrolytes minimize Li depletion and pulverization. *Nature Energy* **2019**, *4*, 796–805.

(49) Zhao, Y.; Zhou, T.; Mensi, M.; Choi, J. W.; Coskun, A. Electrolyte engineering via ether solvent fluorination for developing stable non-aqueous lithium metal batteries. *Nature Communications* **2023**, *14*, 299.

(50) Horowitz, Y.; Han, H.-L.; Ralston, W. T.; de Araujo, J. R.; Kreidler, E.; Brooks, C.; Somorjai, G. A. Fluorinated End-Groups in Electrolytes Induce Ordered Electrolyte/Anode Interface Even at Open-Circuit Potential as Revealed by Sum Frequency Generation Vibrational Spectroscopy. *Advanced Energy Materials* **2017**, *7*, 1602060.

(51) Cao, X.; Gao, P.; Ren, X.; Zou, L.; Engelhard, M. H.; Matthews, B. E.; Hu, J.; Niu, C.; Liu, D.; Arey, B. W.; Wang, C.; Xiao, J.; Liu, J.; Xu, W.; Zhang, J.-G. Effects of fluorinated solvents on electrolyte solvation structures and electrode/electrolyte interphases for lithium metal batteries. *Proceedings of the National Academy of Sciences* **2021**, *118*, e2020357118.

(52) Zhang, Y.; Viswanathan, V. Not All fluorination is the same: Unique effects of fluorine functionalization of ethylene carbonate for tuning solid-electrolyte interphase in Li metal Batteries. *Langmuir* **2020**, *36*, 11450–11466, PMID: 32914986.

(53) von Aspern, N.; Röschenthaler, G.-V.; Winter, M.; Cekic-Laskovic, I. Fluorine and Lithium: Ideal Partners for High-Performance Rechargeable Battery Electrolytes. *Angewandte Chemie - International Edition* **2019**, *58*, 15978 – 16000, Cited by: 142.

(54) Lu, Y.; Tu, Z.; Archer, L. A. Stable lithium electrodeposition in liquid and nanoporous solid electrolytes. *Nature Materials* **2014**, *13*, 961–969.

(55) Amanchukwu, C. V.; Yu, Z.; Kong, X.; Qin, J.; Cui, Y.; Bao, Z. A New Class of Ionically Conducting Fluorinated Ether Electrolytes with High Electrochemical Stability. *Journal of the American Chemical Society* **2020**, *142*, 7393–7403, PMID: 32233433.

(56) Zhang, G.; Deng, X.; Li, J.; Wang, J.; Shi, G.; Yang, Y.; Chang, J.; Yu, K.; Chi, S.-S.; Wang, H., et al. A bifunctional fluorinated ether co-solvent for dendrite-free and long-term lithium metal batteries. *Nano Energy* **2022**, *95*, 107014.

(57) Xu, Z.; Zhang, X.; Yang, J.; Cui, X.; Nuli, Y.; Wang, J.; Wang, C. Multifunctional single-solvent electrolytes for safe and stable Li metal batteries. **2022**,

(58) Ma, P.; Mirmira, P.; Amanchukwu, C. V. Effect of building block connectivity and ion solvation on electrochemical stability and ionic conductivity in novel fluoroether electrolytes. *ACS Central Science* **2021**, *7*, 1232–1244.

(59) Cheng, L.; Assary, R. S.; Qu, X.; Jain, A.; Ong, S. P.; Rajput, N. N.; Persson, K.; Curtiss, L. A. Accelerating electrolyte discovery for energy storage with high-throughput screening. *The journal of physical chemistry letters* **2015**, *6*, 283–291.

(60) Qu, X.; Jain, A.; Rajput, N. N.; Cheng, L.; Zhang, Y.; Ong, S. P.; Brafman, M.; Maginn, E.; Curtiss, L. A.; Persson, K. A. The Electrolyte Genome project: A big data approach in battery materials discovery. *Computational Materials Science* **2015**, *103*, 56–67.

(61) Yao, N.; Chen, X.; Fu, Z.-H.; Zhang, Q. Applying classical, ab initio, and machine-learning molecular dynamics simulations to the liquid electrolyte for rechargeable batteries. *Chemical Reviews* **2022**, *122*, 10970–11021.

(62) Xu, J.; Zhang, J.; Pollard, T. P.; Li, Q.; Tan, S.; Hou, S.; Wan, H.; Chen, F.; He, H.; Hu, E., et al. Electrolyte design for Li-ion batteries under extreme operating conditions. *Nature* **2023**, *614*, 694–700.

(63) Borodin, O.; Ren, X.; Vatamanu, J.; von Wald Cresce, A.; Knap, J.; Xu, K. Modeling insight into battery electrolyte electrochemical stability and interfacial structure. *Accounts of chemical research* **2017**, *50*, 2886–2894.

(64) Mendez-Morales, T.; Li, Z.; Salanne, M. Computational Screening of the Physical Properties of Water-in-Salt Electrolytes. *Batteries & Supercaps* **2021**, *4*, 646–652.

(65) Zhang, Y.; Viswanathan, V. Design rules for selecting fluorinated linear organic solvents for Li metal batteries. *The Journal of Physical Chemistry Letters* **2021**, *12*, 5821–5828.

(66) Chen, Y.; Lee, E. M.; Gil, P. S.; Ma, P.; Amanchukwu, C. V.; de Pablo, J. J. Molecular engineering of fluoroether electrolytes for lithium metal batteries. *Molecular Systems Design & Engineering* **2023**, *8*, 195–206.

(67) Dhattarwal, H. S.; Kuo, J.-L.; Kashyap, H. K. Mechanistic Insight on the Stability of Ether and Fluorinated Ether Solvent-Based Lithium Bis (fluoromethanesulfonyl) Electrolytes near Li Metal Surface. *The Journal of Physical Chemistry C* **2022**, *126*, 8953–8963.

(68) Yang, R. X.; McCandler, C. A.; Andriuc, O.; Siron, M.; Woods-Robinson, R.; Horton, M. K.; Persson, K. A. Big Data in a Nano World: A Review on Computational, Data-Driven Design of Nanomaterials Structures, Properties, and Synthesis. *ACS Nano* **2022**, *16*, 19873–19891, PMID: 36378904.

(69) Tabor, D. P.; Roch, L. M.; Saikin, S. K.; Kreisbeck, C.; Sheberla, D.; Montoya, J. H.; Dwaraknath, S.; Aykol, M.; Ortiz, C.; Tribukait, H., et al. Accelerating the discovery of materials for clean energy in the era of smart automation. *Nature Reviews Materials* **2018**, *3*, 5–20.

(70) Aykol, M.; Herring, P.; Anapolsky, A. Machine learning for continuous innovation in battery technologies. *Nature Reviews Materials* **2020**, *5*, 725–727.

(71) Ahmad, Z.; Xie, T.; Maheshwari, C.; Grossman, J. C.; Viswanathan, V. Machine learning enabled computational screening of inorganic solid electrolytes for suppression of dendrite formation in lithium metal anodes. *ACS central science* **2018**, *4*, 996–1006.

(72) Butler, K. T.; Davies, D. W.; Cartwright, H.; Isayev, O.; Walsh, A. Machine learning for molecular and materials science. *Nature* **2018**, *559*, 547–555.

(73) Jordan, M. I.; Mitchell, T. M. Machine learning: Trends, perspectives, and prospects. *Science* **2015**, *349*, 255–260.

(74) Chen, X.; Liu, X.; Shen, X.; Zhang, Q. Applying machine learning to rechargeable batteries: from the microscale to the macroscale. *Angewandte Chemie* **2021**, *133*, 24558–24570.

(75) Kim, S. C.; Oyakhire, S. T.; Athanitis, C.; Wang, J.; Zhang, Z.; Zhang, W.; Boyle, D. T.; Kim, M. S.; Yu, Z.; Gao, X., et al. Data-driven electrolyte design for lithium metal anodes. *Proceedings of the National Academy of Sciences* **2023**, *120*, e2214357120.

(76) Bultinck, P.; Vanholme, R.; Popelier, P.; De Proft, F.; Geerlings, P. High-speed calculation of AIM charges through the electronegativity equalization method. *The Journal of Physical Chemistry A* **2004**, *108*, 10359–10366.

(77) Lundberg, S. M.; Lee, S.-I. A unified approach to interpreting model predictions. *Advances in neural information processing systems* **2017**, *30*.

(78) Ringsby, A. J.; Fong, K. D.; Self, J.; Bergstrom, H. K.; McCloskey, B. D.; Persson, K. A. Transport Phenomena in Low Temperature Lithium-Ion Battery Electrolytes. *Journal of The Electrochemical Society* **2021**, *168*, 080501.

(79) Rodrigues, M.-T. F.; Babu, G.; Gullapalli, H.; Kalaga, K.; Sayed, F. N.; Kato, K.; Joyner, J.; Ajayan, P. M. A materials perspective on Li-ion batteries at extreme temperatures. *nature energy* **2017**, *2*, 1–14.

(80) Yao, N.; Yu, L.; Fu, Z.-H.; Shen, X.; Hou, T.-Z.; Liu, X.; Gao, Y.-C.; Zhang, R.; Zhao, C.-Z.; Chen, X.; Zhang, Q. Probing the origin of viscosity of liquid electrolytes for lithium batteries. *Angewandte Chemie International Edition* **2023**, e202305331.

(81) Azeez, F.; Fedkiw, P. S. Conductivity of libob-based electrolyte for lithium-ion batteries. *Journal of Power Sources* **2010**, *195*, 7627–7633.

(82) Liu, X.; Zarrabeitia, M.; Mariani, A.; Gao, X.; Schütz, H. M.; Fang, S.; Bizien, T.; Elia, G. A.; Passerini, S. Enhanced Li+ Transport in Ionic Liquid-Based Electrolytes Aided by Fluorinated Ethers for Highly Efficient Lithium Metal Batteries with Improved Rate Capability. *Small Methods* **2021**, *5*, 2100168.

(83) Molinari, N.; Mailoa, J. P.; Craig, N.; Christensen, J.; Kozinsky, B. Transport anomalies emerging from strong correlation in ionic liquid electrolytes. *Journal of Power Sources* **2019**, *428*, 27–36.

(84) Molinari, N.; Mailoa, J. P.; Kozinsky, B. General trend of a negative Li effective charge in ionic liquid electrolytes. *The journal of physical chemistry letters* **2019**, *10*, 2313–2319.

(85) Ruan, D.; Tan, L.; Chen, S.; Fan, J.; Nian, Q.; Chen, L.; Wang, Z.; Ren, X. Solvent versus Anion Chemistry: Unveiling the Structure-Dependent Reactivity in Tailoring Electrochemical Interphases for Lithium-Metal Batteries. *JACS Au* **2023**, *3*, 953–963.

(86) O'Boyle, N. M.; Banck, M.; James, C. A.; Morley, C.; Vandermeersch, T.; Hutchison, G. R. Open Babel: An open chemical toolbox. *Journal of cheminformatics* **2011**, *3*, 1–14.

(87) Neese, F. The ORCA program system. *Wiley Interdisciplinary Reviews: Computational Molecular Science* **2012**, *2*, 73–78.

(88) Lu, T.; Chen, F. Multiwfn: A multifunctional wavefunction analyzer. *Journal of computational chemistry* **2012**, *33*, 580–592.

(89) Humphrey, W.; Dalke, A.; Schulten, K. VMD: visual molecular dynamics. *Journal of molecular graphics* **1996**, *14*, 33–38.

(90) Jorgensen, W. L.; Maxwell, D. S.; Tirado-Rives, J. Development and testing of the OPLS all-atom force field on conformational energetics and properties of organic liquids. *Journal of the American Chemical Society* **1996**, *118*, 11225–11236.

(91) Watkins, E. K.; Jorgensen, W. L. Perfluoroalkanes: Conformational analysis and liquid-state properties from ab initio and Monte Carlo calculations. *The Journal of Physical Chemistry A* **2001**, *105*, 4118–4125.

(92) Chaudhari, M. I.; Nair, J. R.; Pratt, L. R.; Soto, F. A.; Balbuena, P. B.; Rempe, S. B. Scaling atomic partial charges of carbonate solvents for lithium ion solvation and diffusion. *Journal of chemical theory and computation* **2016**, *12*, 5709–5718.

(93) Leontyev, I.; Stuchebrukhov, A. Accounting for electronic polarization in non-polarizable force fields. *Phys. Chem. Chem. Phys.* **2011**, *13*, 2613–2626.

(94) Berendsen, H. J.; van der Spoel, D.; van Drunen, R. GROMACS: A message-passing parallel molecular dynamics implementation. *Computer physics communications* **1995**, *91*, 43–56.

(95) Hess, B. Determining the shear viscosity of model liquids from molecular dynamics simulations. *The Journal of chemical physics* **2002**, *116*, 209–217.

(96) Fong, K. D.; Self, J.; Diederichsen, K. M.; Wood, B. M.; McCloskey, B. D.; Persson, K. A. Ion transport and the true transference number in nonaqueous polyelectrolyte solutions for lithium ion batteries. *ACS central science* **2019**, *5*, 1250–1260.

(97) Liu, H.; Maginn, E. A molecular dynamics investigation of the structural and dynamic properties of the ionic liquid 1-n-butyl-3-methylimidazolium bis (trifluoromethanesulfonyl) imide. *The Journal of chemical physics* **2011**, *135*, 124507.

(98) Gardner, M. W.; Dorling, S. Artificial neural networks (the multilayer perceptron)—a review of applications in the atmospheric sciences. *Atmospheric environment* **1998**, *32*, 2627–2636.

(99) Pedregosa, F.; Varoquaux, G.; Gramfort, A.; Michel, V.; Thirion, B.; Grisel, O.; Blondel, M.; Prettenhofer, P.; Weiss, R.; Dubourg, V., et al. Scikit-learn: Machine learning in Python. *Journal of machine Learning research* **2011**, *12*, 2825–2830.